Fourier space design of high-Q cavities in standard and compressed hexagonal lattice photonic crystals

Kartik Srinivasan and Oskar Painter

Department of Applied Physics, California Institute of Technology, Pasadena, CA 91125, USA.

kartik@caltech.edu

Abstract: Building upon the results of recent work [1], we use momentum space design rules to investigate high quality factor (Q) optical cavities in standard and compressed hexagonal lattice photonic crystal (PC) slab waveguides. Beginning with the standard hexagonal lattice, the results of a symmetry analysis are used to determine a cavity geometry that produces a mode whose symmetry immediately leads to a reduction in vertical radiation loss from the PC slab. The Q is improved further by a tailoring of the defect geometry in Fourier space so as to limit coupling between the dominant Fourier components of the defect mode and those momentum components that radiate. Numerical investigations using the finite-difference time-domain (FDTD) method show significant improvement using these methods, with total Q values exceeding 10^5. We also consider defect cavities in a compressed hexagonal lattice, where the lattice compression is used to modify the in-plane bandstructure of the PC lattice, creating new (frequency) degeneracies and modifying the dominant Fourier components found in the defect modes. High Q cavities in this new lattice geometry are designed using the momentum space design techniques outlined above. FDTD simulations of these structures yield Q values in excess of 10^5 with mode volumes of approximately 0.35 cubic half-wavelengths in vacuum.

OCIS codes: (230.5750) Resonators; (140.5960) Semiconductor lasers

References and links

1. K. Srinivasan and O. Painter, "Momentum space design of high-Q photonic crystal optical cavities," Opt. Express **10,** 670–684 (2002).
2. D. M. Atkin, P. S. J. Russell, T. A. Birks, and P. J. Roberts, "Photonic band structure of guided Bloch modes in high index films fully etched through with periodic microstructure," J. Mod. Opt. **43,** 1035–1053 (1996).
3. S. G. Johnson, S. Fan, P. R. Villeneuve, J. D. Joannopoulos, and L. A. Kolodziejaki, "Guided modes in photonic crystal slabs," Phys. Rev. B **60,** 5751–5758 (1999).
4. S. Noda, A. Chutinan, and M. Imada, "Trapping and emission of photons by a single defect in a photonic bandgap structure," Nature **407,** 608–610 (2000).
5. C. Smith, R. De la Rue, M. Rattier, S. Olivier, H. Benisty, C. Weisbuch, T. Krauss, U. Oesterlé, and R. Houdré, "Coupled guide and cavity in a two-dimensional photonic crystal," Appl. Phys. Lett. **78,** 1487–1489 (2001).
6. O. Painter, K. Srinivasan, J. D. O'Brien, A. Scherer, and P. D. Dapkus, "Tailoring of the resonant mode properties of optical nanocavities in two-dimensional photonic crystal slab waveguides," J. Opt. A **3,** S161–S170 (2001).
7. O. J. Painter, A. Husain, A. Scherer, J. D. O'Brien, I. Kim, and P. D. Dapkus, "Room Temperature Photonic Crystal Defect Lasers at Near-Infrared Wavelengths in InGaAsP," J. Lightwave Tech. **17,** 2082–2088 (1999).

#2009 - $15.00 US Received January 06, 2003; Revised March 15, 2003

8. J. Vučković, M. Lončar, H. Mabuchi, and A. Scherer, "Design of photonic crystal microcavities for cavity QED," Phys. Rev. E 65 (2002).
9. T. Yoshie, J. Vučković, A. Scherer, H. Chen, and D. Deppe, "High quality two-dimensional photonic crystal slab cavities," Appl. Phys. Lett. **79,** 4289–4291 (2001).
10. O. Painter, J. Vučković, and A. Scherer, "Defect Modes of a Two-Dimensional Photonic Crystal in an Optically Thin Dielectric Slab," J. Opt. Soc. Am. B **16,** 275–285 (1999).
11. H. Park, J. Hwang, J. Huh, H. Ryu, Y. Lee, and J. Hwang, "Nondegenerate monopole-mode two-dimensional photonic band gap laser," Appl. Phys. Lett. **79,** 3032–3034 (2001).
12. J. Huh, J.-K. Hwang, H.-Y. Ryu, and Y.-H. Lee, "Nondegenerate monopole mode of single defect two-dimensional triangular photonic band-gap cavity," J. Appl. Phys. **92,** 654–659 (2002).
13. H.-Y. Ryu, S.-H. Kim, H.-G. Park, J.-K. Hwang, Y.-H. Lee, and J.-S. Kim, "Square-lattice photonic band-gap single-cell laser operating in the lowest-order whispering gallery mode," Appl. Phys. Lett. **80,** 3883–3885 (2002).
14. J. Vučković, M. Lončar, H. Mabuchi, and A. Scherer, "Optimization of the Q factor in Photonic Crystal Microcavities," IEEE J. Quan. Elec. **38,** 850–856 (2002).
15. S. G. Johnson, S. Fan, A. Mekis, and J. D. Joannopoulos, "Multipole-cancellation mechanism for high-Q cavities in the absence of a complete photonic band gap," Appl. Phys. Lett. **78,** 3388–3390 (2001).
16. H. Benisty, D. Labilloy, C. Weisbuch, C. Smith, T. Krauss, D. Cassagne, A. Beraud, and C. Jouanin, "Radiation losses of waveguide-based two-dimensional photonic crystals: Positive role of the substrate," Appl. Phys. Lett. **76,** 532–534 (2000).
17. O. Painter and K. Srinivasan, "Localized defect states in two-dimensional photonic crystal slab waveguides: a simple model based upon symmetry analysis," submitted to Phys. Rev. B (2002).
18. O. Painter, K. Srinivasan, and P. E. Barclay, "A Wannier-like Equation for the Resonant Optical Modes of Locally Perturbed Photonic Crystals," submitted to Phys. Rev. B, December 2002.
19. M. Tinkham, *Group Theory and Quantum Mechanics*, *International Series in Pure and Applied Physics* (McGaw-Hill, Inc., New York, NY, 1964).
20. E. Yablonovitch, T. J. Gmitter, R. D. Meade, A. M. Rappe, K. D. Brommer, and J. D. Joannopoulos, "Donor and acceptor modes in photonic band-structure," Phys. Rev. Lett. **67,** 3380–3383 (1991).

1. Introduction

High quality factor (Q) photonic crystal (PC) microcavities are potentially important devices for both lightwave technology and studies in quantum optics. Their ability to confine light to a single resonant mode within an extremely small volume has opened up potential applications for low threshold light sources, ultra-high density planar lightwave circuits, and experiments examining electron-photon interactions in quantum optics. The host geometry for such cavities has typically been a two-dimensional (2D) PC slab waveguide (WG) [2, 3], largely as a result of the maturity of planar fabrication technology. The control exercised by current processing techniques has been evidenced in the ability to integrate PC microresonators with WGs [4, 5], and in the construction of defect cavity lasers with prescribed emission properties [6].

The PC optical microcavities studied in [7] trapped light to a volume of $\approx 2.5(\lambda/2)^3$ in the material [1], nearing the theoretical limit of $(\lambda/2)^3$. The measured Q values were less than 1500, however, and this number must be increased by roughly an order of magnitude or more for PC slab WG microcavities to be favorably compared with their competitors in the applications previously mentioned. Refinements in design [8] and fabrication [9] have further improved the performance of these devices, resulting in predicted Q values of up to 3×10^4 (the highest predicted Q for the designs in [10] was 2×10^4) and measured Q values of up to 2800. At the same time, other types of defect modes have been studied, including a monopole mode in the hexagonal lattice [11, 12] and different types of defect modes in the square lattice [13]. The predicted Q values

[1]This value is quoted in terms of cubic-half wavelengths in the material. Throughout this paper we use the convention that mode volume is to be written in terms of cubic-half wavelengths in *vacuum*. For comparison, the mode volume in terms of vacuum wavelengths of the referenced defect cavity is 0.064.

#2009 - $15.00 US Received January 06, 2003; Revised March 15, 2003

in these structures were also on the order of 10^4, with a measured Q for the monopole mode of $1,900$.

In our previous work [1], we put forth a set of rules for designing high-Q PC slab optical cavities, and considered their application in the design of various defect geometries. The essence of the design is a Fourier space approach to remove those momentum space components that radiate. Using both symmetry and a tailoring of the defect geometry to reduce the presence of these lossy Fourier space components, we were able to design a square lattice defect cavity with $Q{\approx}10^5$ and modal volume $V_{\text{eff}} \approx 0.25(\lambda/2)^3$ in *vacuum*. The work described in this paper is largely an application of the momentum space design rules developed in the earlier work, but now in regards to defect cavities in standard and modified hexagonal lattices. The use of a compressed hexagonal lattice introduces additional degeneracies amongst the satellite extrema of the bandstructure, thus providing the additional design flexibility required to efficiently localized defect modes both vertically and in the plane of the dielectric slab. We begin in Section 2 with a summary of the momentum space design rules previously developed in Ref. [1]. Section 3 includes the preliminary finite-difference time-domain (FDTD) numerical simulation results for the standard hexagonal lattice of Ref. [1], continuing further to consider Fourier space modifications to the dielectric perturbation of the defect cavity. In Section 4, we consider the design of high-Q cavities in a modified hexagonal lattice, where the lattice is compressed in the $\hat{y}$-direction (that is, the spacing between two rows of holes is changed from $a\sqrt{3}/2$ to $\gamma a\sqrt{3}/2$, where a is the original lattice spacing and $\gamma < 1$ is the lattice compression factor). Subsection *4.1* discusses the effects of lattice compression on the in-plane photonic bandstructure, and on the symmetry analysis of defect modes within the lattice. The symmetry analysis is used to choose a mode whose Fourier amplitude is zero at $\mathbf{k} = 0$ (DC), and in subsection *4.2* FDTD results for defect cavities consistent with this symmetry are given.

2. Summary of momentum space design rules

Defect cavities in 2D PC slab WGs confine light through two methods, standard total internal reflection (TIR) in the vertical (waveguiding) direction, and distributed Bragg reflection (DBR) in-plane (Fig. 1). In-plane losses are thus determined by the number of periods in the host photonic lattice and the width and angular extent of the in-plane guided mode bandgap. Vertical confinement is dictated by the condition that the in-plane momentum, $k_\perp$, be sufficiently large to support guiding. To see this, recall that the energy-momentum dispersion relationship for the air cladding of the PC slab WG is given by $(\omega/c)^2 = k_\perp^2 + k_z^2$, where ω is the angular frequency, k_z is the momentum normal to the slab, and c is the speed of light. Examining this equation, we see that $k_\perp^2 = (\omega/c)^2$ defines a cone in (k_x, k_y, ω) space, referred to as the "light cone" of the WG cladding, as illustrated in Fig. 1. At a given ω, for a mode to be guided vertically, $k_\perp > \omega/c$. This is our fundamental guideline in designing cavities that reduce vertical radiation loss.

Before proceeding, let us discuss how this simple rule relates to other methods that have been used to design high-Q PC defect cavities. In addition to our earlier work [1], in Ref. [14], the authors note that a reduction of power within the cladding light cone is a signature for structures with a high vertical Q ($Q_\perp$). The authors tune the geometry of their particular defect geometry to maximize $Q_\perp$, and show that this is reflected by the elimination of small momentum components in the Fourier spectrum of their mode. In Ref. [15], Johnson and co-workers examine the multipole expansion of the radiation field, and demonstrate that a reduction in vertical radiation loss is a result of cancellation of the lower-order components in this expansion. Both in that work and in Ref. [16], delocalization of the field (in-plane in the case of the former work and vertical in the

#2009 - $15.00 US Received January 06, 2003; Revised March 15, 2003

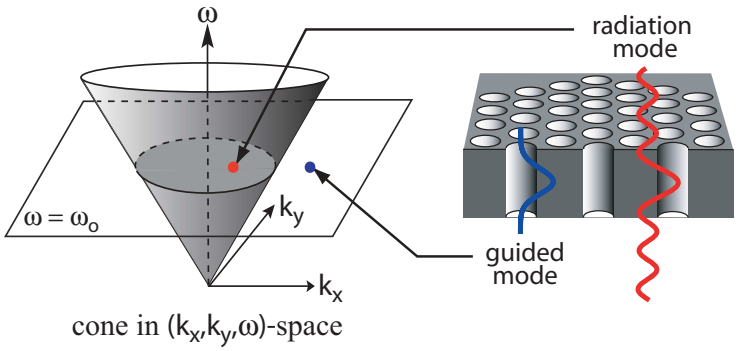

Fig. 1. 2D hexagonal PC slab waveguide structure and cladding light cone.

latter) has also been used as a means for improving $Q_\perp$, as broadening of the mode in real space corresponds to more localized dominant Fourier components in momentum space, thus reducing the presence of power within the cladding light cone. It is important to note that (as discussed in Ref. [1]) methods other than strict delocalization of the field can be used to improve $Q_\perp$. In particular, in that earlier work, we use a tailoring of the defect geometry to improve $Q_\perp$ from $69,000$ to $110,000$ without an appreciable increase in the real-space extent of the field. As was the case in Ref. [1], the approach that we discuss in this article combines several different techniques for improving $Q_\perp$, not all of which rely on delocalization of the field.

Our first step in limiting the presence of small in-plane momentum components is to use symmetry to enforce specific boundary conditions on the Fourier space representation of the mode. In particular, we choose modes whose symmetry is odd about mirror planes normal to the dominant Fourier components of the mode. Within the vertical mirror plane of the slab WG (coordinates $\mathbf{r}_\perp$) the fundamental even (TE-like) modes are described by the field components $\mathbf{E}_x$, $\mathbf{E}_y$, and $\mathbf{B}_z$. Since the magnetic field is exactly scalar within this mirror plane, the criterion reduces to looking for modes in which the magnetic field pattern is spatially even in the directions of its dominant Fourier components, which corresponds to having the in-plane electric field components spatially odd in these directions. In Fourier space, this choice of symmetry is equivalent to eliminating these in-plane electric field polarizations at $\mathbf{k}_\perp = 0$ (DC). This elimination of DC momentum components is the first step in reducing vertical radiation loss, and serves as our criterion for choosing the desired symmetry for our defect mode (note that this use of symmetry to eliminate lossy momentum components can also be viewed as a cancellation of lower-order multipole radiation components, as described in [15]). In order to determine which modes are consistent with the symmetry criterion, we use an approximate group theory analysis (described in [6, 17]) to classify the symmetries of donor and acceptor modes in the lattice under consideration. The process by which this is done is outlined in the following section.

To further improve both in-plane and out-of-plane performance, we consider the mode coupling that is introduced by a defect to a perfect (unperturbed) photonic crystal in Fourier space (a more complete analysis is given in Ref. [18]). Considering the PC slab as an approximately 2D system, and focusing on the fundamental TE-like (even) modes of the slab, reduces the problem to an effective scalar field theory in which the magnetic field is given by $\mathbf{H}(\mathbf{r}) \approx \hat{z}H(\mathbf{r}_\perp)$, with $\mathbf{r}_\perp$ labeling the coordinates within the horizontal plane of the slab (to simplify notation, from here on we drop the $\perp$ label from the in-plane coordinates). The scalar field eigenoperator for the magnetic field in

#2009 - $15.00 US
Received January 06, 2003; Revised March 15, 2003

this quasi-2D approximation is given by,

$$\hat{\mathcal{L}}_H^{\mathrm{TE}} = -\nabla(\eta_o + \Delta\eta)\cdot\nabla - (\eta_o + \Delta\eta)\nabla^2. \tag{1}$$

η_o represents the inverse of the the square of the refractive index of the unperturbed photonic crystal, $1/n_{2\mathrm{D}}^2(\mathbf{r})$, and $\Delta\eta$ is the localized perturbation to $1/n_{2\mathrm{D}}^2(\mathbf{r})$. The mixing of the Bloch modes of the PC due to the presence of the defect perturbation, $\hat{\mathcal{L}}'_H = -\nabla(\Delta\eta)\cdot\nabla - (\Delta\eta)\nabla^2$, can be shown to be given by [18]:

$$\langle H_{l',\mathbf{k}'}|\hat{\mathcal{L}}'_H H_{l,\mathbf{k}}\rangle = \sum_{\mathbf{G}}\sum_{\mathbf{k}''}\Big(\widetilde{\Delta\eta}_{\mathbf{k}''}K_{l',l}(\mathbf{k}',\mathbf{k},\mathbf{G}) + \widetilde{\Delta\eta}_{\mathbf{k}''}(i\mathbf{k}'')\cdot\mathbf{L}_{l',l}(\mathbf{k}',\mathbf{k},\mathbf{G})\Big)\delta_{\mathbf{k}'-\mathbf{k}''+\mathbf{G},\mathbf{k}}, \tag{2}$$

where $\widetilde{\Delta\eta}_{\mathbf{k}''}$ is the $\mathbf{k}''$th Fourier coefficient of $\Delta\eta(\mathbf{r})$, l and $\mathbf{k}$ label the band index and crystal momentum of the $H_{l,\mathbf{k}}$ Bloch wave, and the $\mathbf{G}$ are reciprocal lattice vectors. As shown in Ref. [18], $K_{l',l}(\mathbf{k}',\mathbf{k},\mathbf{G})$ and $\mathbf{L}_{l',l}(\mathbf{k}',\mathbf{k},\mathbf{G})$ are scalar and vector coupling matrix elements, respectively, which depend upon the Bloch waves.

From Eq. (2), it is clear that the Fourier Transform (FT) of the dielectric perturbation, $\widetilde{\Delta\eta}(\mathbf{k})$, is a key quantity in determining the coupling of different Bloch modes of the unperturbed crystal (modulo a reciprocal lattice vector). By tailoring this quantity appropriately, we can thus limit couplings that lead to in-plane and vertical leakage. In particular, we seek to eliminate couplings between a mode's dominant Fourier components and regions of momentum space that are known to radiate, such as the interior of the light cone. Such a tailoring was implemented in Ref. [1] for square photonic lattice defect geometries; we now consider its implementation for standard and compressed hexagonal lattice designs.

3. High-Q defect modes in a hexagonal lattice

For the sake of cogency and completeness, it is worth repeating the results of Ref. [1] for standard hexagonal lattices. In subsection *3.1*, we outline the symmetry classifications for donor and acceptor modes in a hexagonal lattice, and proceed to pick a mode of symmetry consistent with our momentum space design rules of Section 2. A simple defect cavity consistent with this symmetry is simulated through three-dimensional (3D) FDTD methods and results are given. Using this structure as a starting point, subsection *3.2* considers modifications to the dielectric lattice to reduce lossy coupling in Fourier space, and 3D FDTD simulations results are presented.

3.1 Summary of previous results

The real and reciprocal space depictions of a hexagonal PC lattice are given in Fig. 2(a), while its in-plane bandstructure is given in Fig. 2(b). Defect modes are typically classified into donor and acceptor type modes [20], depending upon whether the defect creates modes from the conduction band-edge (the X-point in the hexagonal lattice) or the valence band-edge (the J-point in the hexagonal lattice), respectively. The dominant Fourier components and symmetry of a defect mode are determined by the type of mode (donor or acceptor) under consideration, the symmetry of the surrounding PC lattice, and the point group symmetry of the defect. Candidate modes for high-Q resonators are then chosen from these sets of available modes based upon the criteria placed on the mode's momentum components as described in Section 2.

The high symmetry points in the hexagonal lattice, as indicated in Fig. 2(a), are points a (C_{6v} symmetry), b (C_{2v} symmetry), and c (C_{3v,σ_v} symmetry). We consider

#2009 - $15.00 US Received January 06, 2003; Revised March 15, 2003

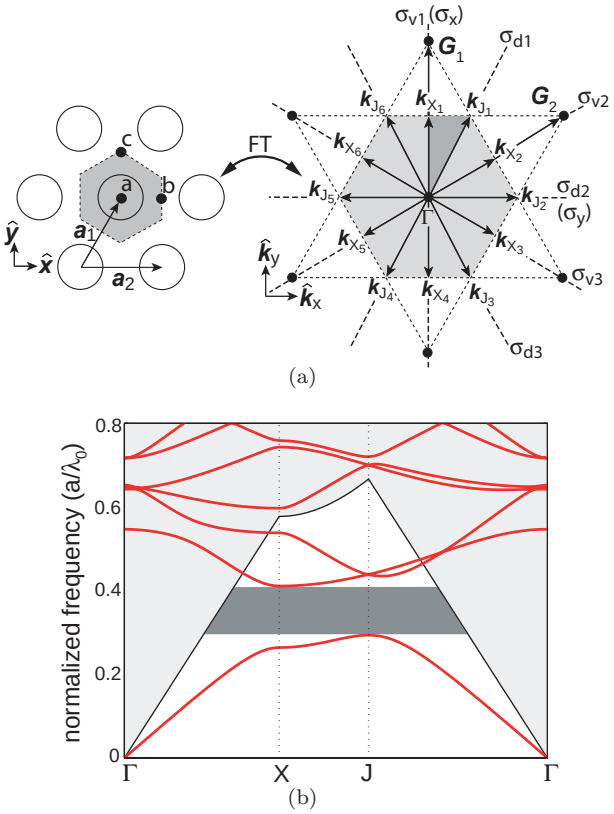

Fig. 2. (a) Real and reciprocal space lattices of a standard 2D hexagonal lattice. Refer to Table 5 for identification of key geometrical quantities. (b) Fundamental TE-like (even) guided mode bandstructure for hexagonal lattice calculated using a 2D plane-wave expansion method with an effective index for the vertical guiding; $r/a = 0.36$, $n_{\text{slab}} = n_{\text{eff}} = 2.65$.

modes formed at points a and b (modes formed from point c are not of the requisite symmetry and dominant Fourier components, as seen from [17]), including reduced symmetry modes formed at point a, where the reduction of symmetry from C_{6v} to C_{2v} is accomplished by choosing a defect that breaks the symmetry of the lattice and is consistent with C_{2v}. Duplicating the results given in Ref. [1], we present Table 1 for donor modes and Table 2 for acceptor modes. These tables provide the labeling scheme for the C_{6v} and C_{2v} modes, the dominant Fourier components of the modes, and their transformation properties about the available mirror planes (the mirror plane properties are represented by their character values [19]).

As discussed in Ref. [1], none of the donor modes presented in the tables above are consistent with our symmetry criteria for reducing vertical radiation losses. Out of the C_{6v} acceptor modes in Table 2, the $\mathbf{B}^{a,a1}_{A''_2}$ mode satisfies the symmetry criteria. For reference, the approximate form for the $\mathbf{B}^{a,a1}_{A''_2}$ mode is listed below [6]:

$$\mathbf{B}^{a,a1}_{A''_2} = \hat{z}\Big(\cos(\mathbf{k}_{J_1}\cdot\mathbf{r}^a_\perp) + \cos(\mathbf{k}_{J_3}\cdot\mathbf{r}^a_\perp) + \cos(\mathbf{k}_{J_5}\cdot\mathbf{r}^a_\perp)\Big), \tag{3}$$

where $\mathbf{r}^a_\perp$ denotes in-plane coordinates referenced to point a.

#2009 - $15.00 US
Received January 06, 2003; Revised March 15, 2003

Table 1. Symmetry classification and dominant Fourier components for the **B**-field of conduction band donor modes in a hexagonal lattice.

Defect Center	C_{6v} Modes	Fourier Comp.	(σ_d, σ_v)[a]	C_{2v} Modes	(σ_x, σ_y)[a]
$(0,0)$	$\mathbf{B}^{a,d1}_{B_1''}$	$\pm\{\mathbf{k}_{X_1}, \mathbf{k}_{X_2}, \mathbf{k}_{X_3}\}$	$(+,-)$	$\mathbf{B}^{a,d1,1}_{B_1}$	$(-,+)$
$(0,0)$	$\mathbf{B}^{a,d1}_{E_1,1}$	$\pm\{\mathbf{k}_{X_1}, \mathbf{k}_{X_2}, \mathbf{k}_{X_3}\}$	$(0,0)$	$\mathbf{B}^{a,d1,2}_{B_1}$	$(-,+)$
$(0,0)$	$\mathbf{B}^{a,d1}_{E_1,2}$	$\pm\{\mathbf{k}_{X_2}, \mathbf{k}_{X_3}\}$	$(0,0)$	$\mathbf{B}^{a,d1}_{B_2}$	$(+,-)$
$(a/2,0)$	N/A[b]	$\pm\{\mathbf{k}_{X_2}, \mathbf{k}_{X_3}\}$	N/A	$\mathbf{B}^{b,d1}_{A_1}$	$(+,+)$
$(a/2,0)$	N/A	$\pm\{\mathbf{k}_{X_2}, \mathbf{k}_{X_3}\}$	N/A	$\mathbf{B}^{b,d1}_{A_2}$	$(-,-)$
$(a/2,0)$	N/A	$\pm\{\mathbf{k}_{X_1}\}$	N/A	$\mathbf{B}^{b,d1}_{B_1}$	$(-,+)$

[a] Character values.
[b] Not Applicable. Modes centered at point b are of C_{2v} symmetry.

Table 2. Symmetry classification and dominant Fourier components for the **B**-field of valence band acceptor modes in a hexagonal lattice.

Defect Center	C_{6v} Modes	Fourier Comp.	(σ_d, σ_v)	C_{2v} Modes	(σ_x, σ_y)
$(0,0)$	$\mathbf{B}^{a,a1}_{A_2''}$	$\pm\{\mathbf{k}_{J_1}, \mathbf{k}_{J_3}, \mathbf{k}_{J_5}\}$	$(-,-)$	$\mathbf{B}^{a,a1}_{A_2}$	$(-,-)$
$(0,0)$	$\mathbf{B}^{a,a1}_{B_2''}$	$\pm\{\mathbf{k}_{J_1}, \mathbf{k}_{J_3}, \mathbf{k}_{J_5}\}$	$(-,+)$	$\mathbf{B}^{a,a1}_{B_2}$	$(+,-)$
$(a/2,0)$	N/A	$\pm\{\mathbf{k}_{J_1}, \mathbf{k}_{J_3}, \mathbf{k}_{J_5}\}$	N/A	$\mathbf{B}^{b,a1}_{A_2}$	$(-,-)$
$(a/2,0)$	N/A	$\pm\{\mathbf{k}_{J_1}, \mathbf{k}_{J_3}, \mathbf{k}_{J_5}\}$	N/A	$\mathbf{B}^{b,a1}_{B_2}$	$(+,-)$

The details of the FDTD calculations presented in this and the following sections were described in Ref. [1], with further information supplied in previous articles [6, 10]. Power flow to vertical and in-plane boundaries have been separated, so that effective Q values $Q_\perp$ and $Q_\parallel$ can be calculated. A normalized slab thickness of $d/a = 0.75$ is typically used in order to ensure a single vertical mode of the PC slab waveguide. Variations in the slab thickness will of course affect both $Q_\parallel$ and $Q_\perp$; in general, we would expect $Q_\perp$ to increase and $Q_\parallel$ to decrease as d/a increases. The increase in $Q_\perp$ is due to the reduced frequency for a defect mode in a thicker slab, as this causes a decrease in the size of the light cone, which determines the degree of vertical radiation loss. The decrease in $Q_\parallel$ is predicted because the in-plane bandgap shrinks in size as the slab thickness increases.

To create the $\mathbf{B}^{a,a1}_{A_2''}$ mode, a central hole (about point a) was enlarged from radius r to r'. The defect is surrounded by a total of 8 periods of the hexagonal lattice in the $\hat{x}$-direction and 12 periods in the $\hat{y}$-direction. The magnetic field amplitude and momentum space electric field components $\widetilde{\mathbf{E}}_x$ and $\widetilde{\mathbf{E}}_y$ of mode $\mathbf{B}^{a,a1}_{A_2''}$ are given in Table 3 for two different pairs of values (r, r'). The dominant Fourier components are seen to be $\pm\{\mathbf{k}_{J_1},\mathbf{k}_{J_3},\mathbf{k}_{J_5}\}$, as predicted by the symmetry analysis. Examining $\widetilde{\mathbf{E}}_x$ and $\widetilde{\mathbf{E}}_y$, it is also clear that, although the power within the light cone has been reduced (in comparison to, say, the x-dipole donor mode, as discussed in Ref. [1]), it is still significant. By reducing the frequency, and consequently the radius of the light cone, the PC cavity with $r/a = 0.30$ and $r'/a = 0.45$ has an improved vertical Q of $8,800$ (although its in-plane Q has degraded due to a reduction in the in-plane bandgap for smaller lattice hole radii).

#2009 - $15.00 US
Received January 06, 2003; Revised March 15, 2003

Table 3. Characteristics of the $\mathbf{B}_{A_2''}^{a,a1}$ resonant mode in a hexagonal lattice (images are for a PC cavity with $r/a = 0.35$, $r'/a = 0.45$, $d/a = 0.75$, and $n_{\text{slab}} = 3.4$).

Geometry	$\lvert\mathbf{B}\rvert$	$\lvert\widetilde{\mathbf{E}}_x\rvert$	$\lvert\widetilde{\mathbf{E}}_y\rvert$
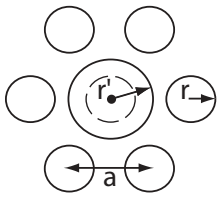	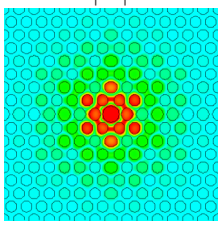	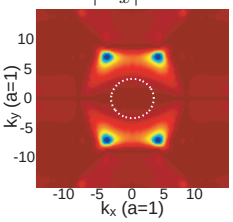	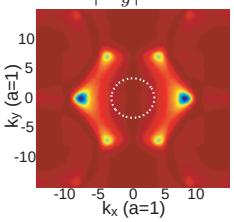

r/a	r'/a	$\omega_n = a/\lambda_o$	$Q_{\parallel}$	$Q_{\perp}$	Q_{tot}	V_{eff}
0.35	0.45	0.265	34,100	4,900	4,300	0.11
0.30	0.45	0.248	5,300	8,800	3,300	0.17

3.2 Tailoring of the defect geometry

When comparing defect modes of a square lattice with those of a hexagonal lattice in the context of forming high-Q microcavities, there are a number of salient points that merit consideration. The first is that the square lattice designs adopted in Ref. [1] provided a natural "geometric" advantage in that $\widetilde{\Delta\eta}(\mathbf{k}_\perp)$ (even in the simplest case of two reduced size air holes) was automatically zero at the dominant Fourier components ($k_x = 0, k_y = \pm\pi/a$), thereby reducing coupling between those components and small momentum components that radiate. Furthermore, these dominant Fourier components were in directions orthogonal to the available mirror planes of the system, maximizing the symmetry-based reduction of small momentum components as discussed in Section 2. In the hexagonal lattice, it is difficult to obtain a similar set of circumstances. The only mode consistent with the symmetry criteria is the $\mathbf{B}_{A_2''}^{a,a1}$ mode, but defects that create such a mode have $\widetilde{\Delta\eta}(\mathbf{k}_\perp)$ that is non-zero at the mode's dominant Fourier components ($\pm\{\mathbf{k}_{J_1},\mathbf{k}_{J_3},\mathbf{k}_{J_5}\}$). Conversely, a mode such as $\mathbf{B}_{A_2}^{b,d1}$, formed by a defect such as two reduced size holes at $(0, \pm a\sqrt{3}/2)$, could have $\widetilde{\Delta\eta}(\mathbf{k}_\perp) = 0$ at its dominant Fourier components ($\pm\{\mathbf{k}_{X_2},\mathbf{k}_{X_3}\}$), but these Fourier components are oriented along directions that are not orthogonal to the available mirror planes of the system.

Despite these obstacles, it is certainly possible to design high-Q defect cavities in a hexagonal lattice. One advantage of the hexagonal lattice is that it exhibits a relatively large and complete in-plane bandgap for TE-like modes due to its nearly circular first Brillouin zone (IBZ) boundary. This essentially guarantees the ability to achieve high in-plane Q provided that the mode is suitably positioned within the bandgap, and that a sufficient number of periods of the photonic lattice are used (it is still important not to entirely neglect in-plane considerations in cavity designs as the mode volume can be affected significantly). To address vertical radiation losses, the defect geometry can be tailored to reduce couplings to the light cone, even though $\widetilde{\Delta\eta}(\mathbf{k}_\perp)$ does not necessarily have the automatic zeros it had in the case of the square lattice. Examining such tailorings is the focus of this section.

Our first goal is to reduce couplings between the dominant Fourier components of the $\mathbf{B}_{A_2''}^{a,a1}$ mode and the light cone. As was demonstrated in Ref. [1], this can be accomplished through a grade in the hole radii as a function of distance from the center of the cavity. In this case, we reduce the hole radius as we move outwards from the

#2009 - $15.00 US
Received January 06, 2003; Revised March 15, 2003

Table 4. FDTD simulation results for graded hexagonal lattice geometries (images are for the first PC cavity listed below; d/a=0.75 in all designs).

Lattice	$\lvert\mathbf{B}\rvert$	$\lvert\widetilde{\mathbf{E}}_x\rvert$	$\lvert\widetilde{\mathbf{E}}_y\rvert$
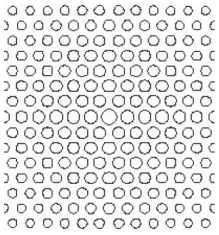	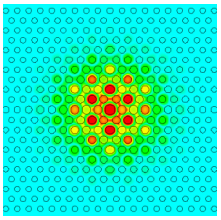	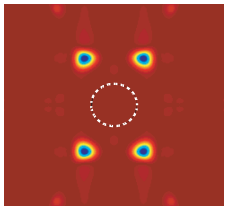	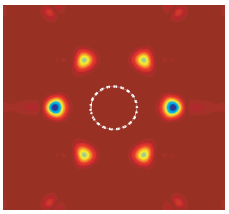

$(r/a)_{\mathrm{c}}$	$(r/a)_{\mathrm{nn}}$	$(r/a)_{\mathrm{e}}$	ω_n	$Q_{\parallel}$	$Q_{\perp}$	Q_{tot}	V_{eff}
0.36	0.325	0.225	0.250	400,000	180,000	123,000	0.49
0.40	0.380	0.30	0.271	1,540,000	76,000	72,000	0.34
0.36	0.355	0.225	0.252	800,000	107,000	94,000	0.24

central defect. An example of a graded lattice defect design is given in Table 4, where only the central region of the cavity is shown to help the reader visualize the hole radii grading (the actual cavity used in FDTD simulations has 10 periods of the hexagonal lattice in each direction). The design consists of two-levels of confinement. The first level of confinement has a centrally enlarged air hole ($(r/a)_{\mathrm{c}} = 0.35$) followed by a relatively large decrease in hole radius ($(r/a)_{\mathrm{nn}} = 0.325$) for the nearest neighbor holes. The hole radii are then parabolically decreased in moving radially outwards (down to $(r/a)_{\mathrm{e}} = 0.225$ at the edge of the crystal), forming the second level of confinement. The effect this has on $\widetilde{\Delta\eta}(\mathbf{k}_{\perp})$ is evident in Fig. 3(a)-(b), where we plot this function for the single enlarged hole design of the previous section and for the graded lattice design just described. It is clear that $\widetilde{\Delta\eta}(\mathbf{k}_{\perp})$ has been dramatically reduced at $\pm\{\mathbf{k}_{J_1},\mathbf{k}_{J_3},\mathbf{k}_{J_5}\}$, limiting the coupling between the dominant Fourier components and the light cone. The magnetic field amplitude and the Fourier transform of the mode's in-plane electric field components are shown in Table 4. The resulting Q values and mode volume, as listed in Table 4, are $Q_{\perp} = 1.8\times10^5$, $Q_{\parallel} = 4\times10^5$, and $V_{\mathrm{eff}} = 0.49$. As previously mentioned, $Q_{\parallel}$ could be made larger by simply increasing the number of periods in the photonic lattice; however, this will not have an appreciable effect on the mode volume, which is somewhat large in this case.

Having achieved a design with a high $Q_{\perp}$, we would like to modify it so as to reduce the mode volume, which, at $V_{\mathrm{eff}} = 0.49$, is roughly twice that which we had for square lattice designs[1]. We employ two different modifications to do so; an increase in the average hole radius and a faster grade in the hole radii (the grading occurs over a smaller number of periods than in the first example), both of which should improve in-plane confinement. The results of these modifications are given in the second row of Table 4; as expected, the in-plane Q has increased considerably, to a value of $Q_{\parallel} = 1.54\times10^6$, and the mode volume has decreased to $V_{\mathrm{eff}} = 0.34$, but at the expense of a decreased vertical Q, now at $Q_{\perp} = 76,000$. The decreased $Q_{\perp}$ is the result of a number of factors. The improved in-plane localization widens the mode in Fourier space, broadening the dominant Fourier components to the extent that they extend into the cladding light cone. The modified grade also changes the magnitude of $\widetilde{\Delta\eta}(\mathbf{k}_{\perp})$ at $\pm\{\mathbf{k}_{J_1},\mathbf{k}_{J_3},\mathbf{k}_{J_5}\}$, increasing the amount of coupling between the mode's dominant Fourier components and the light

#2009 - $15.00 US
Received January 06, 2003; Revised March 15, 2003

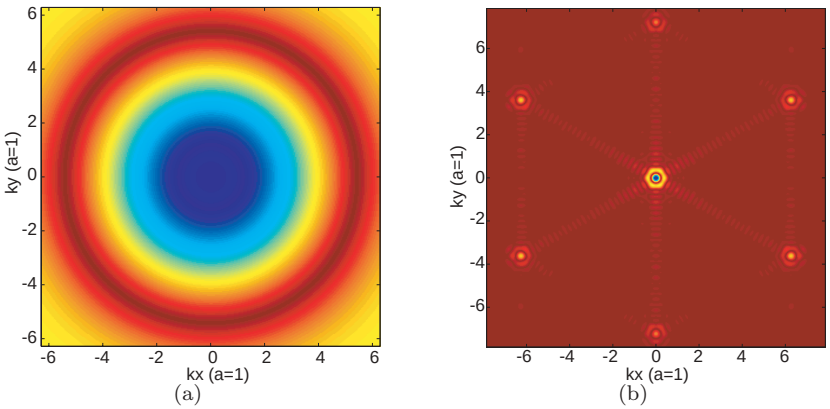

Fig. 3. (a) $\widetilde{\Delta\eta}(\mathbf{k}_\perp)$ for single enlarged hole design in hexagonal lattice ($r/a = 0.30$, $r'/a = 0.45$). (b) $\widetilde{\Delta\eta}(\mathbf{k}_\perp)$ for graded hexagonal lattice design shown in Table 4.

cone. In addition, the increase in modal frequency correspondingly increases the radius of the cladding light cone.

As a final example, we consider adjusting the first level of confinement to reduce the mode volume. Starting with our original graded cavity design (the first design of Table 4), the size of the holes adjacent to the central defect are increased to a value of $(r/a)_{nn} = 0.355$. The results are for the most part intermediate to the first two examples, with $Q_\parallel = 8 \times 10^5$ and $Q_\perp = 1.07 \times 10^5$. One important exception is that $V_{\text{eff}} = 0.24$ is actually much smaller than both of the original designs. Upon further consideration, this result is not too surprising; the smaller mode volume and the relatively large $Q_\perp$ are a result of the stronger yet more extended central perturbation to the photonic lattice.

4. Defect modes in a compressed hexagonal lattice

The defect modes of the previous section were centered about an air hole, and although an experimentally fabricated device with such a design may be useful for certain applications (for example, placing atoms in cavity QED experiments [8]), it is also of interest to have designs centered about a dielectric region, for devices such as lasers, where overlap of the optical field with the semiconductor is necessary. Such a mode would be centered about the b-point in Fig. 2(a). From the standpoint of designing a high-Q mode, the donor and acceptor modes formed at this point do not meet our symmetry criteria, as the dominant Fourier components of the modes (as listed in Tables 1 and 2) are not orthogonal to the available mirror planes (σ_x and σ_y for the C_{2v} symmetry found at the b-point). This is a reflection of the fact that the $\mathbf{k}_{X_i}$ are not mutually orthogonally (nor are the $\mathbf{k}_{J_i}$). Thus, our motivation behind distorting the photonic lattice is to modify the dominant Fourier components of the defect modes, with the potential of creating a mode, centered about the dielectric, whose properties are in accordance with our momentum space design rules.

4.1 Preliminary analysis

We would like to create a mode whose dominant Fourier components are orthogonal to σ_x and σ_y. Such a mode would have dominant Fourier components $\pm\mathbf{k}_{X_1}$ and/or $\pm\mathbf{k}_{J_2}$. Let us begin by considering acceptor modes. By compressing the lattice in the $\hat{y}$-direction, so that the spacing between two adjacent rows of holes is less than its usual value (changing it from $a\sqrt{3}/2$ to $\gamma a\sqrt{3}/2$, where γ is the compression factor),

#2009 - $15.00 US
Received January 06, 2003; Revised March 15, 2003

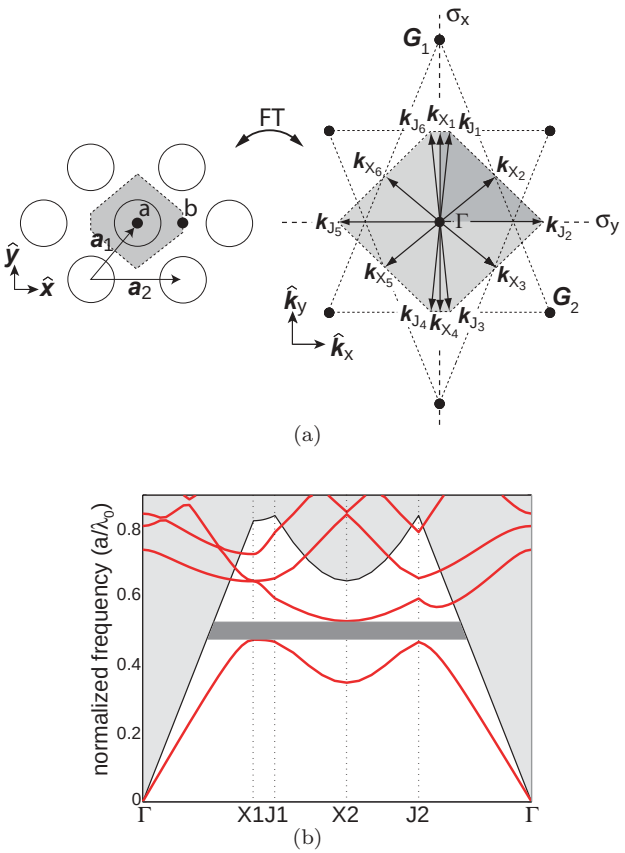

Fig. 4. (a) Real and reciprocal space lattices of a compressed 2D hexagonal lattice. Refer to Table 5 for more identification of key geometrical quantities; (b) Fundamental TE-like (even) guided mode bandstructure for a compressed hexagonal lattice, calculated using a 2D plane-wave expansion method with an effective index for the vertical guiding; $r/a = 0.35$, $n_{\text{slab}} = n_{\text{eff}} = 2.65$, $\gamma = 0.7$.

we intuitively expect the position of the band edges in that direction of Fourier space (corresponding to $\pm\mathbf{k}_{X_1}$) to increase in frequency, perhaps to the point where the valence band-edge at X_1 is nearly degenerate with the valence band-edge at the J-points. Of course, this qualitative justification leaves many questions unanswered (such as the position of the band-edges at the other high symmetry points in the lattice). To properly answer these questions, we formulate a symmetry analysis of defect modes in compressed hexagonal lattices, using the methods of [6, 17].

Consider the real and reciprocal space representations of the compressed hexagonal lattice as illustrated in Fig. 4(a). Compression has reduced the point group symmetry of the lattice to C_{2v}, and the irreducible Brillouin zone (IrBZ) is no longer a $30°-60°-90°$ triangle, but is now a quadrilateral, traced between $\Gamma - X_1 - J_1 - X_2 - J_2 - \Gamma$. The modifications in various geometrical quantities associated with the real and reciprocal space compressed lattice are given in Table 5. Note that, in particular, the group of the wavevector $\mathcal{G}_{o\mathbf{k}}$ at the X and J points has been reduced in symmetry, and that $|\mathbf{k}_{X_1}| \neq |\mathbf{k}_{X_2}|$ (the $\mathbf{k}_{J_i}$ are still equal in magnitude). Furthermore, $|\mathbf{k}_{X_1}|$ now approaches $|\mathbf{k}_J|$. Indeed, for a compression factor $\gamma = 1/\sqrt{3}$, the vectors coincide and the resulting lattice is in fact square. For compression factors between 0.8 and $1/\sqrt{3}$, the vectors are

#2009 - $15.00 US
Received January 06, 2003; Revised March 15, 2003

still quite close in magnitude, and we qualitatively expect that the lowest frequency band (the valence band) will be very nearly degenerate at the X_1 and J points. It is in this way that the compressed hexagonal lattices considered in this section are intermediate to the hexagonal and square lattices. In using the compressed hexagonal lattice we hope to take advantage of the large in-plane bandgap of the hexagonal lattice and the favorable symmetry of the square lattice.

Table 5. Key geometrical quantities associated with the standard and compressed hexagonal lattices.

Crystal Parameter(s)	Hexagonal Lattice	Compressed Hexagonal Lattice
$\mathcal{G}_a$ [a]	C_{6v}	C_{2v}
$\mathcal{G}_b$ [b]	C_{2v}	C_{2v}
$\{\mathbf{a}_1, \mathbf{a}_2\}$	$\{(\frac{a}{2}, \frac{a\sqrt{3}}{2}), (a, 0)\}$	$\{(\frac{a}{2}, \frac{a\sqrt{3}\gamma}{2}), (a, 0)\}$
$\{\mathbf{G}_1, \mathbf{G}_2\}$	$\{(0, \frac{4\pi}{a\sqrt{3}}), (\frac{2\pi}{a}, -\frac{2\pi}{a\sqrt{3}})\}$	$\{(0, \frac{4\pi}{a\sqrt{3}\gamma}), (\frac{2\pi}{a}, -\frac{2\pi}{a\sqrt{3}\gamma})\}$
$\pm X_1$	$(0, \pm\frac{2\pi}{a\sqrt{3}})$	$(0, \pm\frac{2\pi}{a\sqrt{3}\gamma})$
$\pm X_2$	$(\pm\frac{\pi}{a}, \pm\frac{\pi}{a\sqrt{3}})$	$(\pm\frac{\pi}{a}, \pm\frac{\pi}{a\sqrt{3}\gamma})$
$\pm X_3$	$(\pm\frac{\pi}{a}, \mp\frac{\pi}{a\sqrt{3}})$	$(\pm\frac{\pi}{a}, \mp\frac{\pi}{a\sqrt{3}\gamma})$
$\pm J_1$	$(\pm\frac{2\pi}{3a}, \pm\frac{2\pi}{a\sqrt{3}})$	$(\pm\frac{\pi}{a}(1 - \frac{1}{3\gamma^2}), \pm\frac{2\pi}{a\sqrt{3}\gamma})$
$\pm J_2$	$(\pm\frac{4\pi}{3a}, 0)$	$(\pm\frac{\pi}{a}(1 + \frac{1}{3\gamma^2}), 0)$
$\pm J_3$	$(\pm\frac{2\pi}{3a}, \mp\frac{2\pi}{a\sqrt{3}})$	$(\pm\frac{\pi}{a}(1 - \frac{1}{3\gamma^2}), \mp\frac{2\pi}{a\sqrt{3}\gamma})$
$\mathcal{G}_{o,\mathbf{k}_{X_i}}$ [c]	C_{2v}	C_{2v}
$\mathcal{G}_{o,\mathbf{k}_{J_1}}$	C_{3v}	$C_{1v} = \{e, \sigma_y\}$
$\mathcal{G}_{o,\mathbf{k}_{J_2}}$	C_{3v}	$C_1 = \{e\}$
$\mathcal{G}_{o,\mathbf{k}_{J_3}}$	C_{3v}	$C_{1v} = \{e, \sigma_y\}$

[a] Point Group for defect at point a of lattice.
[b] Point Group for defect at point b of lattice.
[c] Group of the wavevector.

Using the 2D plane wave expansion method with an effective index to account for vertical waveguiding ([10]), we arrive at the bandstructure shown in Fig. 4(b). The compression ratio (γ) has been set at a value of 0.7 for this calculation. We see that the valence band is nearly degenerate at points X_1, J_1, and J_2, and thus, we expect an acceptor mode to be formed by mixing the valence band modes formed at all of these points in Fourier space. Following the symmetry analysis techniques originally described in [6], we determine approximate forms for valence band modes at these points. Grouping all of them together, we arrive at the following expressions for modes formed about the high symmetry point a shown in Fig. 4(a):

$$VB_a = \hat{z} \begin{pmatrix} \cos(\mathbf{k}_{X_1} \cdot \mathbf{r}_\perp^{\mathbf{a}}) \\ e^{-i\mathbf{k}_{J_1}\cdot\mathbf{r}_\perp^a} + e^{-i\mathbf{k}_{J_3}\cdot\mathbf{r}_\perp^a} \\ e^{-i\mathbf{k}_{J_4}\cdot\mathbf{r}_\perp^a} + e^{-i\mathbf{k}_{J_6}\cdot\mathbf{r}_\perp^a} \\ e^{-i\mathbf{k}_{J_2}\cdot\mathbf{r}_\perp^a} \\ e^{-i\mathbf{k}_{J_5}\cdot\mathbf{r}_\perp^a} \end{pmatrix} \tag{4}$$

#2009 - $15.00 US Received January 06, 2003; Revised March 15, 2003

Note that the valence band modes formed about the high symmetry point b (found by taking $\mathbf{r}_\perp^b = \mathbf{r}_\perp^a - \mathbf{b}$) differ from these only by constant phase factors and hence the modes above can be used for investigations about b as well. Both the a and b points have C_{2v} symmetry, and the representation of the VB_a basis under C_{2v}, labeled $S^{a,a1}$, is given by $S^{a,a1} = 3A_2 \oplus 2B_2$, where A_2 and B_2 label irreducible representations (IRREPs) of C_{2v}. In our previous analyses, we were able to take such a representation and use projection operators on the basis functions to get approximate forms for the localized modes. In this case, we have no such luxury, as there is no way to distinguish between the modes of the different A_2 (or B_2) subspaces without some additional physical knowledge of the system. The best we can do is to form one projection operator for a composite A_2 subspace and another for a composite B_2 subspace. Doing so yields the following matrices, where the rows and columns are ordered in accordance with that which was chosen for the VB_a modes above:

$$P_{A_2} = \begin{pmatrix} 2 & 0 & 0 & 0 & 0 \\ 0 & 1 & 1 & 0 & 0 \\ 0 & 1 & 1 & 0 & 0 \\ 0 & 0 & 0 & 1 & 1 \\ 0 & 0 & 0 & 1 & 1 \end{pmatrix}, \qquad P_{B_2} = \begin{pmatrix} 0 & 0 & 0 & 0 & 0 \\ 0 & 1 & -1 & 0 & 0 \\ 0 & -1 & 1 & 0 & 0 \\ 0 & 0 & 0 & 1 & -1 \\ 0 & 0 & 0 & -1 & 1 \end{pmatrix}. \tag{5}$$

By the form of these projection matrices, it is clear that the A_2 modes can potentially be formed from any of the degenerate band-edge points $\{\pm\mathbf{k}_{X_1}, \pm\mathbf{k}_{J_1}, \pm\mathbf{k}_{J_2}, \pm\mathbf{k}_{J_3}\}$, while the B_2 modes do not include $\pm\mathbf{k}_{X_1}$. It is our hope to design defects that produce A_2 modes which only contain $\pm\mathbf{k}_{X_1}$ and $\pm\mathbf{k}_{J_2}$, to satisfy our symmetry criteria from Section 2. To see if this can be the case, in the next section we consider FDTD simulations of defect cavities in this lattice.

Before moving on to discuss FDTD simulations, for the sake of completeness, let us briefly consider donor modes in this lattice. Such modes will be formed from the conduction band-edge located at point X_2 in Fig. 4(b). Using a symmetry analysis similar to that described above, we determine the conduction band modes for the a and b high symmetry points:

$$CB_a = \hat{z}\begin{pmatrix} \sin(\mathbf{k}_{X_2} \cdot \mathbf{r}_\perp^{\mathbf{a}}) \\ \sin(\mathbf{k}_{X_3} \cdot \mathbf{r}_\perp^{\mathbf{a}}) \end{pmatrix}, \qquad CB_b = \hat{z}\begin{pmatrix} \cos(\mathbf{k}_{X_2} \cdot \mathbf{r}_\perp^{\mathbf{b}}) \\ \cos(\mathbf{k}_{X_3} \cdot \mathbf{r}_\perp^{\mathbf{b}}) \end{pmatrix}, \tag{6}$$

where $\mathbf{r}_\perp^b = \mathbf{r}_\perp^a - \mathbf{b}$.

The representation of the CB_a basis under C_{2v} (the defect symmetry), labeled $S^{a,d1}$, is given by $S^{a,d1} = B_1 \oplus B_2$, while the representation of the CB_b basis under C_{2v}, labeled $S^{b,d1}$ is given by $S^{b,d1} = A_1 \oplus A_2$. Projecting the CB_a and CB_b bases onto the irreducible representations above, we get

$$\begin{aligned} \mathbf{B}_{B_1}^{a,d1} &= \hat{z}\Big(\sin(\mathbf{k}_{X_2} \cdot \mathbf{r}_\perp^a) - \sin(\mathbf{k}_{X_3} \cdot \mathbf{r}_\perp^a)\Big), \\ \mathbf{B}_{B_2}^{a,d1} &= \hat{z}\Big(\sin(\mathbf{k}_{X_2} \cdot \mathbf{r}_\perp^a) + \sin(\mathbf{k}_{X_3} \cdot \mathbf{r}_\perp^a)\Big), \\ \mathbf{B}_{A_1}^{b,d1} &= \hat{z}\Big(\cos(\mathbf{k}_{X_2} \cdot \mathbf{r}_\perp^b) - \cos(\mathbf{k}_{X_3} \cdot \mathbf{r}_\perp^b)\Big), \\ \mathbf{B}_{A_2}^{b,d1} &= \hat{z}\Big(\cos(\mathbf{k}_{X_2} \cdot \mathbf{r}_\perp^a) + \cos(\mathbf{k}_{X_3} \cdot \mathbf{r}_\perp^b)\Big), \end{aligned} \tag{7}$$

as approximate forms for the donor modes at points a and b.

#2009 - $15.00 US
Received January 06, 2003; Revised March 15, 2003

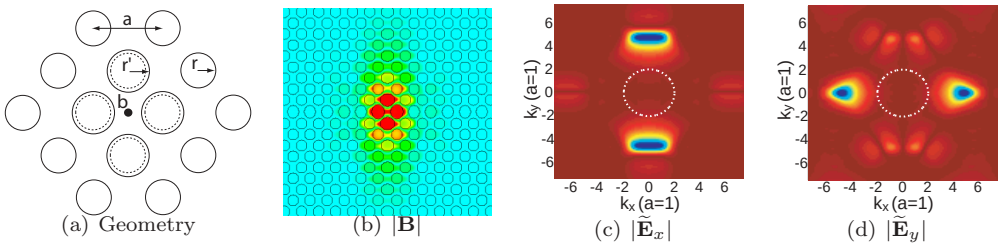

(a) Geometry (b) $|\mathbf{B}|$ (c) $|\widetilde{\mathbf{E}}_x|$ (d) $|\widetilde{\mathbf{E}}_y|$

Fig. 5. Modal characteristics of a simple defect mode in a compressed hexagonal lattice ($d/a = 0.75$).

4.2 FDTD results

As discussed in the previous sections, we are interested in forming an A_2 symmetry mode in the compressed hexagonal lattice, centered about the b-point, whose dominant Fourier components are situated at $\{\pm\mathbf{k}_{X_1}, \pm\mathbf{k}_{J_2}\}$, to be consistent with the symmetry criterion we have prescribed. The group theory analysis just presented has indicated that the modes of the correct symmetry are acceptor-type modes, and have $\{\pm\mathbf{k}_{X_1}, \pm\mathbf{k}_{J_1}, \pm\mathbf{k}_{J_2}, \pm\mathbf{k}_{J_3}\}$ as their potential dominant Fourier components. We thus begin our FDTD design in the compressed hexagonal lattice by analyzing the dominant Fourier components produced by a simple defect geometry.

Consider the defect geometry depicted in Fig. 5(a), consisting of four enlarged holes surrounding the b-point in a compressed hexagonal lattice with compression factor $\gamma = 0.7$. FDTD simulations of such a design (choosing, for example, $r/a = 0.30$ and $r'/a = 0.35$), give the magnetic field amplitude and Fourier transformed dominant electric field components shown in Fig. 5(b)-(d). We see that our defect geometry has produced a mode with dominant Fourier components centered at $\{\pm\mathbf{k}_{X_1}, \pm\mathbf{k}_{J_2}\}$, as desired. Having produced a mode consistent with our symmetry criterion, our next step is to tailor the defect geometry so as to produce a high-Q mode.

The procedure followed is the same as what has been done in the square and hexagonal lattices, namely, we modify the lattice (and therefore $\widetilde{\Delta\eta}(\mathbf{k}_\perp)$) to reduce couplings between the mode's dominant Fourier components (in this case, $\{\pm\mathbf{k}_{X_1}, \pm\mathbf{k}_{J_2}\}$) and the light cone. We do so by starting with a defect consisting of the four enlarged holes surrounding the b-point (we choose $r'/a = (r/a)_{\mathrm{c}} = 0.30$), and then parabolically decreasing the hole radius as we move away from the defect center (down to a value of $(r/a)_{\mathrm{e}} = 0.225$ at the edge of the crystal). The resulting lattice is shown in Table 6 (only the central region has been shown; in total there are 10 periods of air holes in $\hat{x}$ and 8 periods in $\hat{y}$ surrounding the defect center), along with the magnetic field amplitude and Fourier transformed electric field components for the defect mode. FDTD calculations predict $Q_\perp = 1.5\times10^5$, $Q_\parallel = 7.5\times10^5$, $Q_{tot} = 1.3\times10^5$, and $V_{\mathrm{eff}} = 0.35$ for this design.

The modifications to the lattice have largely accomplished our objectives, as we have simultaneously achieved high vertical and in-plane Qs, while keeping the modal volume reasonably small (although this value is still larger than our previous designs). Improvements can still be made; for example, simulation results indicate that there are still momentum components present within the light cone of $\widetilde{\mathbf{E}}_y$; hence a further tailoring of the lattice in the $\hat{x}$-direction ($\widetilde{\mathbf{E}}_y$ has its dominant Fourier components along $\pm\mathbf{k}_{J_2}$) should help increase $Q_\perp$, though potentially at the expense of a larger mode volume.

#2009 - $15.00 US
Received January 06, 2003; Revised March 15, 2003

Table 6. FDTD simulation results for graded compressed hexagonal lattice geometries.

Lattice	$\lvert\mathbf{B}\rvert$	$\lvert\widetilde{\mathbf{E}}_x\rvert$	$\lvert\widetilde{\mathbf{E}}_y\rvert$
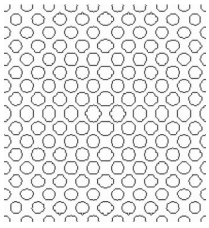	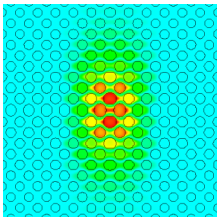	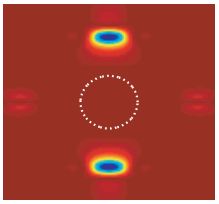	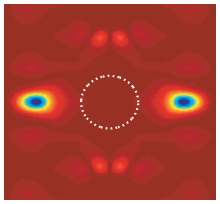

$(r/a)_{\mathrm{c}}$	$(r/a)_{\mathrm{e}}$	ω_n	$Q_{\parallel}$	$Q_{\perp}$	Q_{tot}	V_{eff}
0.30	0.225	0.323	755,000	152,000	127,000	0.35

5. Summary

The design of high-Q defect modes in a 2D PC slab WG through Fourier space methods, as discussed in Ref. [1], has been investigated for defects in hexagonal and compressed hexagonal lattice geometries. The primary design methods employed are: (i) the choice of the mode's symmetry so that it is odd about mirror planes orthogonal to the mode's dominant Fourier components, and (ii) a tailoring of the defect geometry to avoid momentum space couplings that lead to loss. These tools are first applied to a candidate acceptor mode in a standard hexagonal lattice, and successfully produce designs with Qs in excess of 10^5. As this mode is centered about an air hole, we seek out a mode centered about a dielectric region for applications where modal overlap with the dielectric is an important asset. To be consistent with our symmetry criterion, which precluded using such a mode in the standard hexagonal lattice, we consider a compression of the lattice in the $\hat{y}$-direction as a method for creating new band-edge degeneracies which then alter the dominant Fourier components present in the defect modes. The symmetry-based analysis [6, 17] previously used to identify candidate high-Q modes in square and hexagonal lattices is applied to this new lattice, and FDTD simulations of defect geometries tailored to reduce lossy momentum space couplings predict $Q's$ exceeding 10^5 with a modal volume $V_{\mathrm{eff}} \approx 0.35$. Including the results of Ref. [1] for the square lattice, we have used the Fourier space guidelines to design high-Q cavities in three different lattices, indicating the generality of this Fourier space-based approach.

K. Srinivasan thanks the Hertz Foundation for its financial support.

#2009 - $15.00 US
Received January 06, 2003; Revised March 15, 2003